Assessment of Remote Sensing Technologies for Location of Hydrogen and Helium Leaks

NAG10-0290

Phase 1 Final Report

28 February 2000

R. Glenn Sellar
Danli Wang

This research was supported by the NASA Kennedy Space Center
under grant # NAG10-0290

Florida Space Institute

TABLE OF CONTENTS

1 EXECUTIVE SUMMARY

The objective of this initial phase of this research effort is to:

- Evaluate remote sensing technologies for location of leaks of gaseous molecular hydrogen (H_2) and gaseous helium (He) in air, for space transportation applications.
- Develop a diffusion model that predicts concentration of H_2 or He gas as a function of leak rate and distance from the leak.

The hierarchy of techniques for H_2 and He leak location is shown in Figure 2. The hierarchy shown in Figure 2 illustrates the comprehensive nature of this study. By beginning our exploration of the range of possible techniques at topmost level of the hierarchy, and then working down through subcategories to the individual techniques, we ensure that the study encompasses the broadest and most complete range of possible approaches. In a sense Figure 2 might be considered a comprehensive *roadmap* to possible techniques.

The topmost division in the hierarchy is between *in-situ* techniques and *remote* techniques. An in-situ technique is one that measures *at* the location of the sensor, while a remote technique is one that makes a measurement at some distance away from the sensor itself. The objective of this project is to evaluate remote techniques only. In-situ techniques are by definition outside the scope of this project.

At the bottom level of the hierarchy a total of twelve specific techniques are selected for more detailed evaluation:

- Passive Sonar
- Active Sonar
- Differential Absorption Lidar (DIAL)
- Fourier Transform Infrared Spectroscopy (FTIR)
- Spontaneous Raman spectroscopy
- Stimulated Raman Scattering (SRS)
- Coherent Anti-Stokes Raman Spectroscopy (CARS)
- Rayleigh Doppler
- Indirect Thermal
- Rayleigh Intensity
- Schlieren Imaging
- Shearography

For each technique, the principle is briefly described, and a bibliography is provided listing references that describe the technique in detail. The applicability for location of H_2 and He leaks is discussed for each technique, with emphasis on the sensitivity, spatial resolution, and constraints (cost, size, field of view, ease of use, etc.) Quantitative models for expected performance are included for most of the techniques. The technological maturity of each technique for application to location of H_2 and He leaks is assessed in

terms of the appropriate NASA Technology Readiness Level (TRL). The results of these evaluations are summarized in Figure 2.

An interactive diffusion model has been developed using MathCAD. For diffusion into a large area, the concentration is given by:

$$C(r,t) = \frac{\phi}{4\pi Dr} efrc\left[\frac{r}{\sqrt{4Dt}}\right]$$

where C is the concentration [mol fraction] (equivalent to volume fraction), t is the time since initiation of the leak, ϕ is the leak rate [mol/s], D is the diffusion coefficient for the gas in air [m^2/s], r is the distance from the leak [m], and *erfc* is the *complimentary error function*.

Sample results from the MathCAD model are given in Figure 1, which shows the molar fraction in percent (equivalent to percent concentration by volume) as a function of distance from the leak for an H_2 leak at 10^{-2} SCIM after 1 s, 1 min, 1 h, and for steady state.

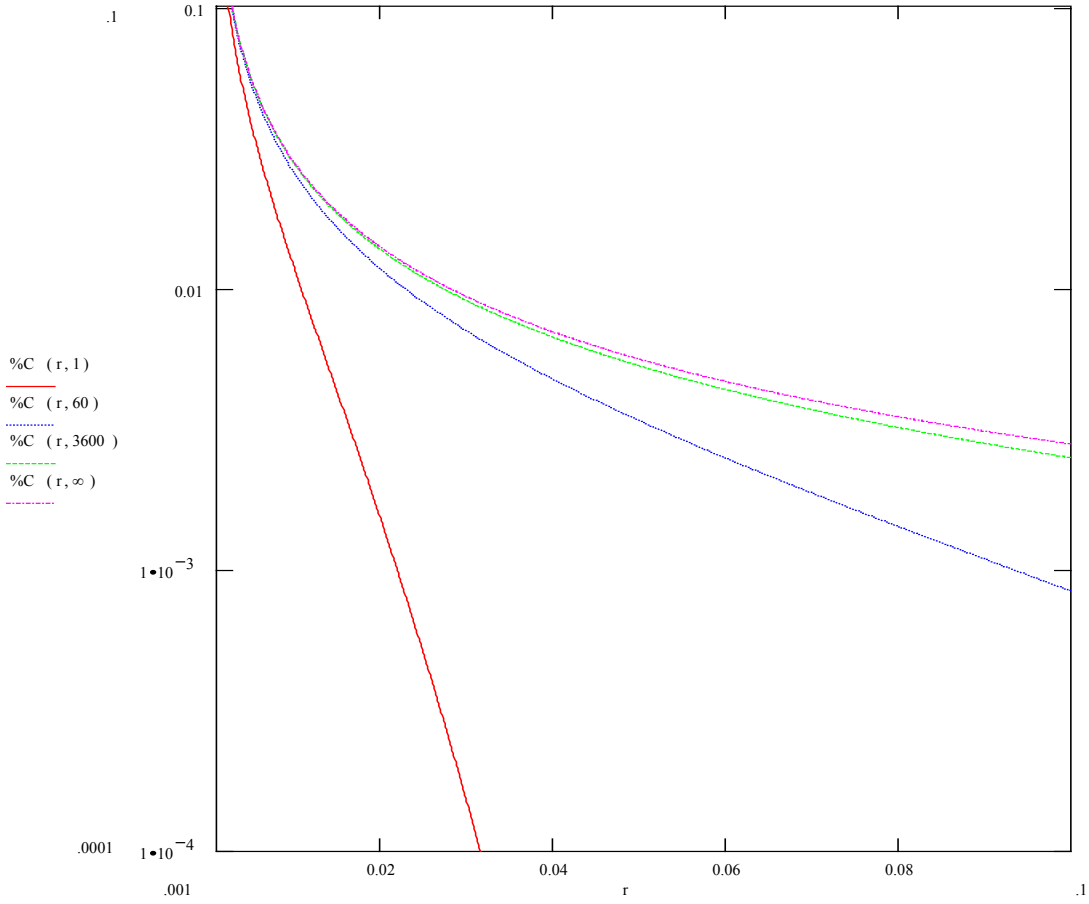

Figure 1: Concentration of H_2 [mol fraction] vs. distance [m] for a leak of 10^{-2} SCIM, at 1 s, 1 min, 1 h, and steady state

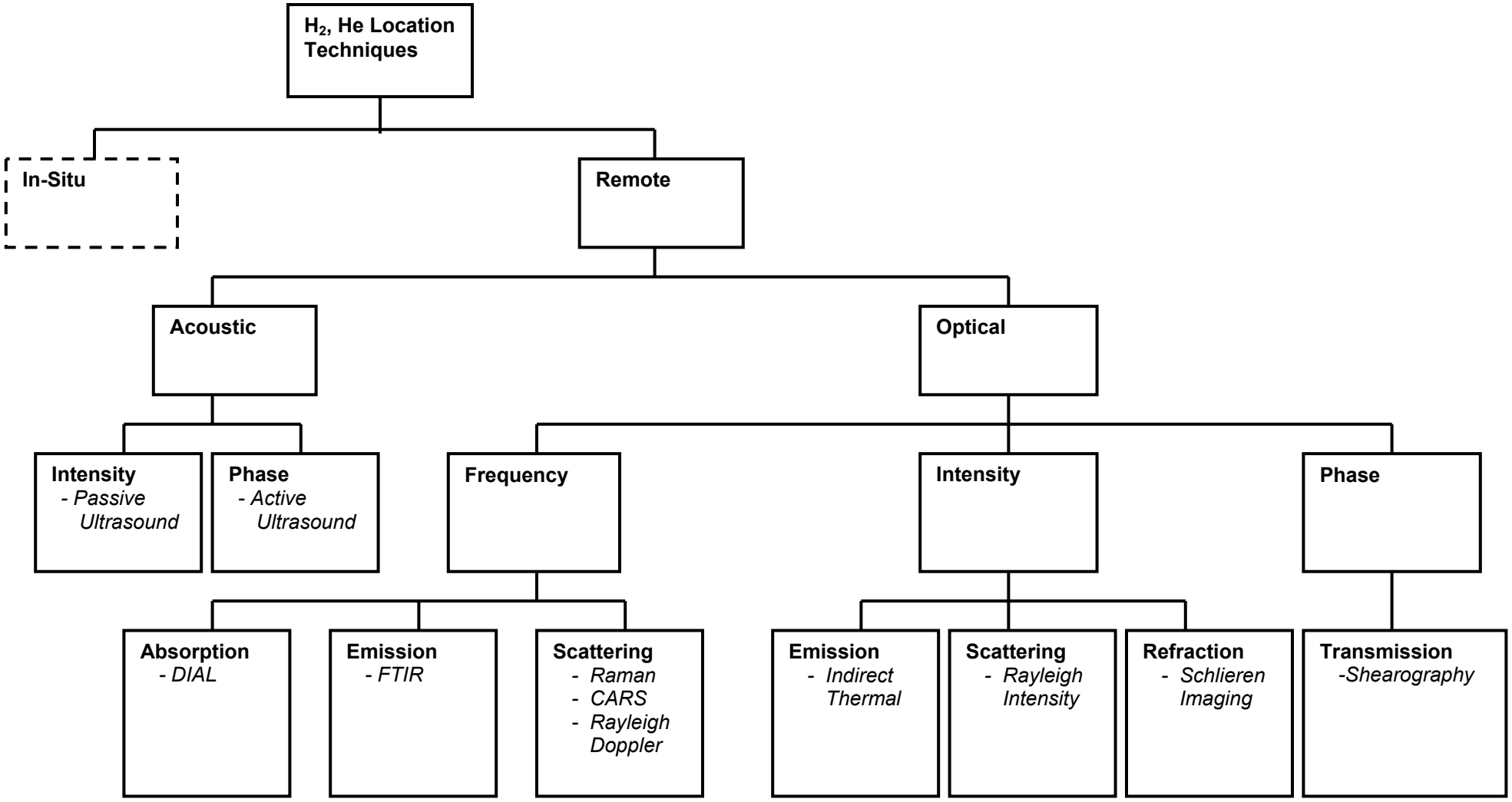

Figure 2: Hierarchy of H_2 & He Location Techniques

Table 1: Technology Evaluation Summary

Technique	**Distinguishing Characteristic**	**Measurement**	**Applicability**	**TRL**
Passive Sonar	Turbulent airflow (ultrasound)	Acoustic intensity (passive)	Demonstrated Low spatial resolution Sensitivity depends on pressure and aperture	4
Active Sonar	Speed of sound	Phase of acoustic waves (active)	Low spatial resolution Sensitivity limited by clutter	3
DIAL	Allowable energy levels	Absorption of radiation at characteristic wavelengths (active)	None – absorption lines only in vacuum UV	-
FTIR	Allowable energy levels	Emission of radiation at characteristic wavelengths (passive)	None – absorption lines only in vacuum UV	-
Raman - spontaneous	Allowable energy levels	Shift in wavelength of inelastically scattered radiation (active)	H_2: Sensitivity of 2% demonstrated *He*: None – monatomic therefore no vibration	6
Raman – CARS	Allowable energy levels	Shift in wavelength of inelastically scattered radiation (active)	H_2: Sensitivity of 10 ppm demonstrated *He*: None – monatomic therefore no vibration	3
Rayleigh Doppler	Molecular/atomic velocities	Shift in wavelength of elastically scattered radiation (active)	Theoretically applicable for both H_2 and He	1
Indirect Thermal	Temperature	Variation in temperature of solids caused by nearby cryogenic gas or expanding gas (passive)	Clutter limited?	3
Rayleigh Intensity	Molecular/atomic cross-section	Intensity of elastically scattered radiation (active)	Limited by Mie scattering (particulates) Clutter limited?	3
Schlieren	Index of refraction	Refraction of radiation caused by spatial variations in index of refraction (active)	Sensitivity limited by clutter: 1° ~ 346 ppm H_2 1° ~ 461 ppm He	4
Shearography	Index of refraction	Phase (path length) of transmitted radiation (active)	Sensitivity limited by clutter: 1° ~ 346 ppm H_2 1° ~ 461 ppm He	5

2 INTRODUCTION

Figure 2 shows the hierarchy of techniques for location of H_2 and He leaks in air. The topmost division in the hierarchy shown in Figure 2 is between *in-situ* techniques and *remote* techniques. An in-situ technique is one that measures *at* the location of the sensor, while a remote technique is one that makes a measurement at some distance away from the sensor itself. The objective of this project is to evaluate remote techniques only. In-situ techniques are by definition outside the scope of this project.

The second level division is between different *signal carriers*. For a sensor to make a measurement at some distance from the sensor itself, 'something' must travel from the point of measurement to the sensor. *Acoustic* techniques use sound as a signal carrier, while *optical* techniques use electromagnetic radiation (i.e. light or microwaves.)

The third level divisions are based on the property of the carrier that is measured. As both sound and electromagnetic radiation are wavelike in nature, the property measured may be the *frequency*, the *intensity*, or the *phase*. The acoustic frequency subcategory is omitted from Figure 2, since the type of gas has no effect on the frequency of a sound wave, to our knowledge.

The fourth level divisions are based on the nature of the interaction between the carrier and the gas. Sound or electromagnetic radiation may interact by absorption, emission, scattering, refraction or transmission. Subcategories for which there is no distinction between different gases, to our knowledge, have been omitted from the figure.

Finally, within each bottom-level subcategory we list one or more specific techniques based on that particular interaction. These comprise the twelve techniques studied in more detail in this project. While we do not claim these particular twelve techniques to be the only feasible techniques; we do believe that the hierarchy presented here encompasses all feasible techniques. In a sense, Figure 2 might be considered a comprehensive *roadmap* to possible techniques.

3 TECHNOLOGY ASSESSMENTS

3.1 Passive Sonar

3.1.1 Principle of Operation

Depending upon the pressure differential and the size and geometry of the orifice through which a gas is leaking, the leak may create a turbulent flow or 'jet'. The resulting turbulent pressure variations can be detected by an acoustic sensor or *sonar* system. This signal may span a range of frequencies, but is typically strongest in the neighborhood[1,2] of 40 kHz. Since this is above the frequency range of human hearing, this technique is also known as *ultrasound*.

If the sensor is made to be directional in nature then information on the location of the leak may be obtained. This can be achieved in practice by either using an array of sensors or by scanning a single sensor. The directional selectivity can be achieved with a baffle or a curved reflector. This is a passive technique, as the leak itself is the acoustic source.

3.1.2 Quantitative Model

The intensity and frequency spectrum of the sound signal is a complicated function of the pressure differential and the geometry of the orifice. Models for these parameters are not included in this report, but it is expected that analytical fluid dynamics techniques should be able to predict these parameters for orifices with simple shapes. Computational fluid dynamics techniques may allow modeling of these parameters to some extent for orifices with more general shapes.

The angular resolution limit for this technique is given approximately by:

$$\theta \approx \frac{\lambda}{D}$$

where θ is the angular resolution limit in radians, λ is the wavelength of the sound wave, and D is the diameter of the collector.

3.1.3 Application to Location of Hydrogen and Helium Leaks

The passive sonar technique is applicable to both H_2 and He leaks. The two principal limitations are:

1) The leak must create sufficient turbulent pressure variations. High pressure and a small orifice will tend to satisfy this condition, while low pressure or a large orifice may not.
2) The angular resolution is limited by the wavelength of the sound waves and the size of the baffle or reflector. This limits the precision with which the leak may be located. For example, for a frequency of 40 kHz and a diameter of 30 cm the angular resolution limit is 1.6°. At a range of 2 m this corresponds to a spatial resolution of approximately 6 cm.

3.1.4 Technology Readiness Level

A prototype detector has been constructed and successfully tested in a laboratory environment, so the maturity is assessed as TRL 4.

3.1.5 Bibliography

- Youngquist, et al. “Ultrasonic imaging system”, United States Patent: 5,979,239. November 9, 1999. (see Appendix 6.2.1)
- Youngquist, et al. “Ultrasonic leak detection system”, United States Patent: 5,710,377. January 20, 1998. (see Appendix 6.2.2)

3.2 Active Sonar

3.2.1 Principle of Operation

The speed of sound in a gas is different for different gases or mixtures of gases. This speed may be determined by measuring the time of travel for an acoustic pulse or the phase of a continuous acoustic signal. If the acoustic sensors are directionally selective, then a *sonar image* may be created. This is an active technique (an acoustic source must be provided). The source and detector may be located on opposite sides of the test volume, or together on one side of the test volume. If the source and detector are co-located, the signal must be reflected by a solid background. In this latter case would be a more practical set-up, useable in a broader range of environments, but the image would show the shape of the background so it would only be possible to detect *changes* in the gas mixture.

3.2.2 Quantitative Model

The speed of sound is dramatically different for air, H_2 and He (see Table 2.)

Table 2: Speed of sound for air, H_2, and He

Gas	Speed of sound at 1 atm, 20 C [m/s]
air	344
H_2	1339
He	927

The speed of sound in all three gases varies as a function of temperature and pressure.

The variation as a function of temperature and pressure for air is given by:

$$V_s = \sqrt{\gamma \cdot R \cdot T}$$

Where V_s is the speed of sound, γ is ratio of the specific heats (1.4 for air at STP,) R is the gas constant (286 $m^2/s^2/K$ for air,) and T is absolute temperature (K).

The speed of sound in a mixture of these gases is expected to be in the range between the speeds for the pure gases.

3.2.3 Application to Location of Hydrogen and Helium Leaks

The addition of H_2 or He to air will change the speed of sound in the resulting mixture, so this technique is applicable to both H_2 and He leaks.

The sensitivity of this technique is expected to be limited by clutter. Variations in the speed of sound will result from variations in the temperature of the ambient air, even

where no H_2 or He is present. It may be possible to distinguish a leak from this clutter from a leak from the context (i.e. a jet-shaped disturbance extending from a seal or joint may be identified as a leak.) But the extent to which this would be effective is difficult to quantify. A definitive answer to this would best be obtained by actual testing in the appropriate operation environment.

The angular resolution limitation for this technique is the same as for the passive sonar (ultrasound) technique (see section 3.1).

3.2.4 Technology Readiness Level

Sonar technology in general is quite mature, and experimental work has demonstrated the ability of this technique to to detect refractive index variations in air[12]. So the maturity is assessed as TRL 3.

3.2.5 Bibliography

- Youngquist, et al. "Ultrasonic imaging system", United States Patent: 5,979,239. November 9, 1999. (see Appendix 6.2.1)
- Youngquist, et al. "Ultrasonic leak detection system", United States Patent: 5,710,377. January 20, 1998. (see Appendix 6.2.2)
- Glenn Research Center, "Speed of Sound" http://www.grc.nasa.gov/WWW/K-12/airplane/sound.html (Sep.2000)
- http://www.cudenver.edu/public/chemistry/classes/LabNet/Sound/pages/compressibility

3.3 Differential Absorption Lidar

3.3.1 Principle of Operation

Gases absorb electromagnetic radiation (e.g. light) of some wavelengths much more strongly than other wavelengths. The wavelengths at which a gas absorbs strongly is characteristic of the gas, and thus may be used to distinguish between gases. These wavelengths are determined by the allowed electronic energy levels, allowed vibrational energy levels, and allowed rotational energy levels for the atoms or molecules of each particular gas.

Differential absorption lidar (DIAL) systems scan a laser beam including two or more distinct wavelengths over a volume of gas and measure the intensity that returns to a detector co-located with the laser source. If a gas is present that absorbs one of the wavelengths, then the intensity of the return at that wavelength will be weak compared to that at another wavelength. The ratio of these intensities is an indicator of amount of absorbing gas present along the line of sight of the laser and detector system. The source and detector system are scanned to create a two-dimensional image of the gas concentration. In most implementations a third dimension (range) is also obtained, by using a pulsed laser source and measuring the time of travel for each pulse.

3.3.2 Quantitative Model

Quantitative models for DIAL exist, but since this technique is not applicable to locating H_2 or He in air (see section 3.3.3), these models are not included in this report.

3.3.3 Application to Location of Hydrogen and Helium Leaks

The wavelengths at which a gas absorbs are determined by the allowed electronic energy levels, allowed vibrational energy levels, and allowed rotational energy levels for the atoms or molecules of each particular gas. Transitions between allowed electronic energy levels cause absorption at visible and ultraviolet wavelengths. Transitions between allowed vibrational energy levels cause absorption at infrared wavelengths. Transitions between allowed rotational energy levels cause absorption at far infrared and microwave wavelengths.

Only molecules have vibrational or rotational energy levels. Single atoms (such as He) lack these transitions. An additional condition for significant absorption due to vibrational or rotational transitions is that the molecule must have a dipole moment. Molecules formed of two of the same type of atoms – such as H_2 – have no dipole moment and thus do not significantly absorb due to vibrational or rotational transitions.

3.3.3.1 Hydrogen

The wavelengths at which H_2 absorbs[3,4] are all in the *vacuum ultraviolet*, the region of the ultraviolet spectrum that is strongly absorbed by air. Therefore the DIAL technique is not applicable for location of H_2 in air.

3.3.3.2 Helium

The wavelengths at which He absorbs[5] are also all in the vacuum ultraviolet. Therefore this technique is not applicable for location of He in air.

3.3.4 Technology Readiness Level

Since this approach is not suitable for location of H_2 or He in air, the application, the TRL is not applicable.

3.3.5 Bibliography

- Robert P. Bruno, "Tracking Gas Leaks With Active IR Scanning: Laser and imager combine to detect hazardous gases from leaking tanks and other sources", *Photonics Spectra,* Pp. 94 – 98, February 1992. (see Appendix 6.2.3)
- Gerhard Herzberg, F.R.S. 1989, *Molecular Spectra and Molecular Structure: Volume I. Spectra of Diatomic Molecules,* 2nd Edition, Pp.54 & 279, Malabar: Krieger.
- Owen Willans Richardson, *Molecular Hydrogen and Its Spectrum,* p. 65, New Haven: Yale University Press.

3.4 Fourier Transform Infrared

3.4.1 Principle of Operation

Gases may emit electromagnetic radiation at discrete wavelengths that are characteristic of the gas. *These wavelengths are the same as those at which the gas absorbs* (see section 3.3). The intensity of these emissions depends primarily on the wavelength and the temperature of the gas. For gases at room temperature or colder, significant intensities occur only for the infrared wavelengths.

An infrared spectrometer may be used to measure the wavelengths that are emitted, and thus enable gases to be identified. The most suitable type of spectrometer for this is the Fourier Transform Spectrometer, which lends its name to the technique of FTIR (Fourier Transform Infrared). Imaging versions of this spectrometer may allow gases to be located as well as identified.

3.4.2 Quantitative Model

Quantitative models for FTIR exist, but since this technique is not applicable to locating H2 or He in air (see section 3.4.3), these models are not included in this report.

3.4.3 Application to Location of Hydrogen and Helium Leaks

3.4.3.1 Hydrogen

The wavelengths at which H_2 emits[3,4] are all in the vacuum ultraviolet. Significant emission at these wavelengths only occurs if the gas is extremely hot, and in these wavelengths would be strongly absorbed by air. Therefore the FTIR technique is not applicable for location of H_2 in air.

3.4.3.2 Helium

The wavelengths at which He emits[5] are all in the vacuum ultraviolet. Therefore this technique is not applicable for location of He in air.

3.4.4 Technology Readiness Level

Since this approach is not suitable for location of H_2 or He in air, the application, the TRL is not applicable.

3.4.5 Bibliography

- Gerhard Herzberg, F.R.S. 1989, *Molecular Spectra and Molecular Structure: Volume I. Spectra of Diatomic Molecules,* 2nd Edition, Pp.54 & 279, Malabar: Krieger.
- Owen Willans Richardson, *Molecular Hydrogen and Its Spectrum,* p. 65, New Haven: Yale University Press.

3.5 Spontaneous Raman Scattering

3.5.1 Principle of Operation

When electromagnetic radiation is scattered off of a molecule, the scattered radiation has two components: most of the radiation is elastically scattered radiation, while a small portion is inelastically scattered and shifted in wavelength due to an exchange of vibrational energy to or from the molecule. The elastic scatter is known as *Rayleigh* scatter while the inelastic is known as *Raman* scattering. The magnitudes of these shifts in wavelength are characteristic of the composition of the molecule, and measurement of this shift is known as *Raman spectroscopy*.

In the most common implementation of Raman spectroscopy, a laser is used as the source and a monochromator (or a double- or triple-monochromator) is used to separate the Raman radiation from the stronger Rayleigh component and send it to a detector array. If measurement of the wavelength of the scattered radiation is not required, a simple filter and a single detector may be used for separation and measurement, respectively. *Raman lidar* systems have been demonstrated[6], which scan the laser beam and detector in elevation and azimuth. If the laser is pulsed, and the time of flight is measured, then resolution in a third dimension (range) may also be obtained.

3.5.2 Quantitative Model

For a spontaneous Raman system the number of photons received by the detector is given by[6]:

$$N_{pe} = E \times (h\upsilon)^{-1} \times C(1\%) \times \sigma_R \times L \times R^{-2} \times A \times \varepsilon_0 \times \varepsilon_f \times \varepsilon_{pe}$$

where:

N_{pe} is the number of photoelectrons detected.

E is the energy of the laser in Joules.

$(h\upsilon)^{-1}$ is the number of photons per Joule at the laser wavelength.

$C(1\%)$ is the gas concentration, 1% used for computation.

σ_R is the cross section for Raman scattering at the laser wavelength in.

L is the path length over which scattering is observed.

R is the distance from the target to the detector in meters.

A is the area of the detector in meter^2.

ε_0 is the optical efficiency of the detector.

ε_f is the transmission efficiency of the detector.

ε_{pe} is the photoelectric conversion efficiency of the detector.

Values of σ_R are given in Table 3 for various laser wavelengths.

Table 3: Raman cross-sections for various laser wavelengths

laser wavelength [nm]	248	266	308	337	355	532
σ_R [cm^2/ster]	$4.5\text{x}10^{-29}$	$3.4\text{x}10^{-29}$	$1.89\text{x}10^{-29}$	$1.32\text{x}10^{-29}$	$1.07\text{x}10^{-29}$	$2.1\text{x}10^{-30}$

The intensity of each Raman line as observed with a spectroscopic system is given by[7]:

$$I_R = I_0 C N_{V'J'} \nu_R^4 \left\langle \alpha \right\rangle_{fj}^2$$

where:

I_0 is the intensity of the incident laser

$N_{V'J'}$ is the number of molecules with an initial energy state that generates this Raman line described by vibration and rotational quantum number V$'$ and J$''$.

C is a constant which includes the solid angle over which the Raman radiation is collected, the efficiency of the collection optics and the spectral response of the detector.

υ_R is the frequency of the Raman line.

$\left\langle \alpha \right\rangle_{fj}^2$ is the transition probability or the probability that a molecule within the molecular population $N_{V'J'}$ radiates light under the influence of laser irradiation at frequency υ_R.

The subscripts f and j indicate the final and initial energy state.

The frequency of any Raman line is given by[7]:

$$\nu_R = \nu_0 \pm \left[\left(E_{V'J'} - E_{V''J''} \right) / h \right]$$

where:

ν_R is the position (frequency) of the Raman signal

ν_0 is the frequency of the laser light

$E_{V'J'}$ is the initial rotational-vibrational energy level state

$E_{V''J''}$ is the final rotational-vibrational energy level state

h is Planck's constant, which is equal to 6.62×10^{-34} J·s

3.5.3 Application to Location of Hydrogen and Helium Leaks

Unlike emission and absorption, Raman scattering does not require that the molecule have a natural dipole moment (see section 3.3.3 and 3.4.3), since the incident electromagnetic radiation can induce a dipole moment. Therefore this technique is applicable to molecules with no dipole moment, such as H_2. Detection of H_2 at a partial pressure of 2 kPa (~2% of 1 atm) has been demonstrated in the laboratory[7] using this technique.

It is generally required, however, that the molecule have vibrational and/or rotational modes. A single atom (such as He) will therefore not exhibit vibrational or rotational Raman spectra.

Consequently, this technique is applicable to location of H_2 leaks in air, but not to location of He leaks in air.

3.5.4 Technology Readiness Level

Field tests of Raman lidar systems for location of H_2 have been carried out at Stennis Space Center[8] in 1988, and at Johnson Space Center[9] in 1990, so this technology is assessed as TRL 6.

3.5.5 Bibliography

- Wim A. de Groot, "The use of Spontaneous Raman Scattering for Hydrogen Leak Detection", NASA CR 195373, AIAA-94-2983 (1994). (see Appendix 6.2.4)
- "Evaluation of Raman Lidar For Hydrogen Detection", NASA Report # 802841. (see Appendix 6.2.5)
- "Lidar Hydrogen Detection Test", NASA Transmitting Station No. 4963 (Jan., 28, 1991). (see Appendix 6.2.6)
- E. Roland Menzel, *Laser Spectroscopy: Techniques and Application*, New York: Marcel Dekker, (1995).
- John R. Ferraro and Kazuo Nakamoto, "Introductory Raman Spectroscopy", San Diego: Academic Press (1994).
- "Raman Lidar Testing at JSC, DRAFT", (Nov. 5, 1990). (see Appendix 6.2.7)
- D. Kirk Veirs and Gerd M. Rosenblatt, "Raman Line position in Molecular Hydrogen: H_2, HD, HT, D_2, DT, and T_2", *Journal of Molecular Spectroscopy,* **121** (1987).

3.6 Coherent Anti-Stokes Raman Scattering

3.6.1 Principle of Operation

Raman scattering occurs when the electric field of the incident electromagnetic radiation polarizes the molecule (induces a dipole moment). The electric polarization P induced in a molecule by an applied electric field E can be represented by a polynomial[10]:

$$P \cong E\chi + E^2\chi' + E^3\chi''$$

where χ , χ', and χ'' are the first, second and third order dielectric susceptibilities. The higher-order susceptibilities are relatively small, so at low field strengths, the linear (first order) term dominates. This first-order polarization results in spontaneous Raman scattering. At higher field strengths, the higher-order terms dominate and non-linear Raman scattering effects occur. The non-linear dependence has two effects: it produces Raman scattered radiation of high enough strength to produce significant stimulated radiation (which is highly directional as in a laser beam), and it allows multiple oscillating electric fields (electromagnetic radiation) to interact in affecting the polarization of the molecules. The possible interactions of radiation of one, two, three or four colors produces a wide variety of what are referred to as non-linear Raman effects, including: stimulated Raman gain (SRG), inverse Raman scattering (IRS), Raman-induced Kerr effect spectroscopy (RIKES), and coherent anti-Stokes Raman spectroscopy (CARS).

The CARS technique is particularly useful for analyses of gases, due to two advantages:

1) The non-linear dependence makes it possible to achieve Raman signal levels many orders of magnitude stronger than those for spontaneous Raman, and
2) The coherent nature of the Raman radiation in CARS allows for very efficient collection of the signal, in contract to spontaneous Raman where the scattered radiation is spread in all directions.

3.6.2 Quantitative Model

The anti-Stokes intensity I_3 is given by[11]:

$$I_3 = \left(16\pi^4/c^4\right)\omega_3^2\left|\chi\right|^2 I_1^2 I_2 z^2$$

where z is the distance traveled into the medium by waves ω_1 and ω_2 with intensities I_1 and I_2 respectively, and χ is the Raman susceptibility. The latter is complex and can be expanded as[11]:

$$\chi = \chi' + i\chi'' + \chi^{nr}$$

Where χ^{nr} is the nonresonant electronic contribution. At or near resonance, χ' vanishes ; χ'' can be expressed as $\chi = N\gamma/\Delta\omega$, where N is the molecular number density and, $\Delta\omega$ is

the Raman linewidth, and $\gamma/\Delta\omega$ is the amplitude of the susceptibility per molecule. The parameter γ is related to the differential Raman scattering cross section $d\sigma/d\Omega$ by[11]:

$$\gamma = \frac{\pi c^4}{\hbar \omega_2^3 \omega_1} \frac{d\sigma}{d\Omega}$$

3.6.3 Application to Location of Hydrogen and Helium Leaks

As for the spontaneous Raman technique, this technique is not applicable to He, since single atoms do not exhibit vibrational or rotational Raman spectra (see section 3.5.3).

The CARS technique is quite sensitive for measurement of the concentration of H_2. Detection of concentrations of H_2 in air as low as 10 ppm has been demonstrated in the laboratory[11]. This sensitivity limit results from the background signal from the N_2. For this technique, however, the scattered radiation is confined to a cone at a small angle of deflection relative to the incident beam. This requires that the laser source and the detector system be placed on opposite sides of the volume of interest. And since this is a non-linear technique, with a third-power dependence on the incident intensity, a high intensity is required to obtain a signal. CARS systems typically focus the incident laser beam on a roughly cylindrical volume that is ~ 1mm in diameter and a few mm long. In order to use such a system for leak location the laser beam and detecting system would need to scan over the volume of interest.

3.6.4 Technology Readiness Level

While this technique has been demonstrated in the laboratory for measurement of H_2 concentration in a fixed volume of a few mm in size, it has not been demonstrated for location of H_2 in a large volume. So the technology readiness level is assessed as TRL 3.

3.6.5 Bibliography

- W. M. Tolles, J.W. Nibler, J.R. McDonald, and A.B. Harvey, "A Review of the Theory and Application of Coherent Anti-Stokes Raman Spectroscopy (CARS)", *Applied Spectroscopy,* Vol.31, No.4, (1977). (see Appendix 6.2.8)
- P.R. Regnier, and J.P.-E.Taran, "On the possibility of measuring gas concentrations by stimulated anti-Stokes scattering", *Appl. Phys. Lett.,* Vol.23, No. 5, (1973). (see Appendix 6.2.9)
- *Chemical Applications of Nonlinear Raman Spectroscopy*, Albert B. Harvey *ed.*, Naval Research Laboratory: Washington, D.C. (1981).

3.7 Rayleigh Doppler

3.7.1 Principle of Operation

As discussed in section 3.5.1, when electromagnetic radiation (e.g. light) interacts with a molecule it may be scattered elastically or inelastically. In the elastic case, referred to as *Rayleigh* scattering, there is no interaction with the electronic, vibrational or rotational energy of the molecule. In the inelastic case, referred to as *Raman* scattering, there *is* interaction with the electronic, vibrational or rotational energy of the molecule.

In addition to electronic, vibrational and rotational energy, however, a molecule may also have kinetic energy, due to motion of the molecule as a whole. When electromagnetic radiation is emitted, scattered, or reflected from an object moving toward or away from an observer, the observed wavelength is shifted in what is known as the *Doppler* effect. Thus the Rayleigh scattered radiation may be shifted in wavelength due to the velocity of the scattering molecules.

Velocity v is related to kinetic energy E_k, according to the following equation:

$$E_k = \frac{1}{2}mv^2$$

where m is the mass of the molecule and v is its velocity. The distribution of kinetic energies of the molecules in a gas is independent of the *type* of molecules of which the gas is comprised, and depends only on the temperature of the gas. But since different molecular species have different masses, the distribution of *velocities* will vary with the composition of the gas.

Since the molecules in a gas move in a random distribution of directions, when light of a single frequency is scattered from a gas, the spectrum of the scattered light is broadened in an effect known as *Doppler broadening*. The degree of broadening will be dependent on the velocities of the molecules, which in turn depends upon the composition of the gas. Thus it may be possible to determine the composition of a gas by measuring the Doppler broadening of Rayleigh scattered light[12].

3.7.2 Quantitative Model

The distribution of velocities in a gas is given by the Maxwell-Boltzmann distribution:

$$f(v) = 4\pi\left(\frac{m}{2\pi kT}\right)^{\frac{3}{2}} v^2 e^{\frac{-mv^2}{2kT}}$$

where m is the mass of the molecule, k is the Stephan-Boltzmann constant, and T is the absolute temperature. The velocity distributions for H_2, He, N_2 and O_2 at 293 K (room temperature) are shown in Figure 3.

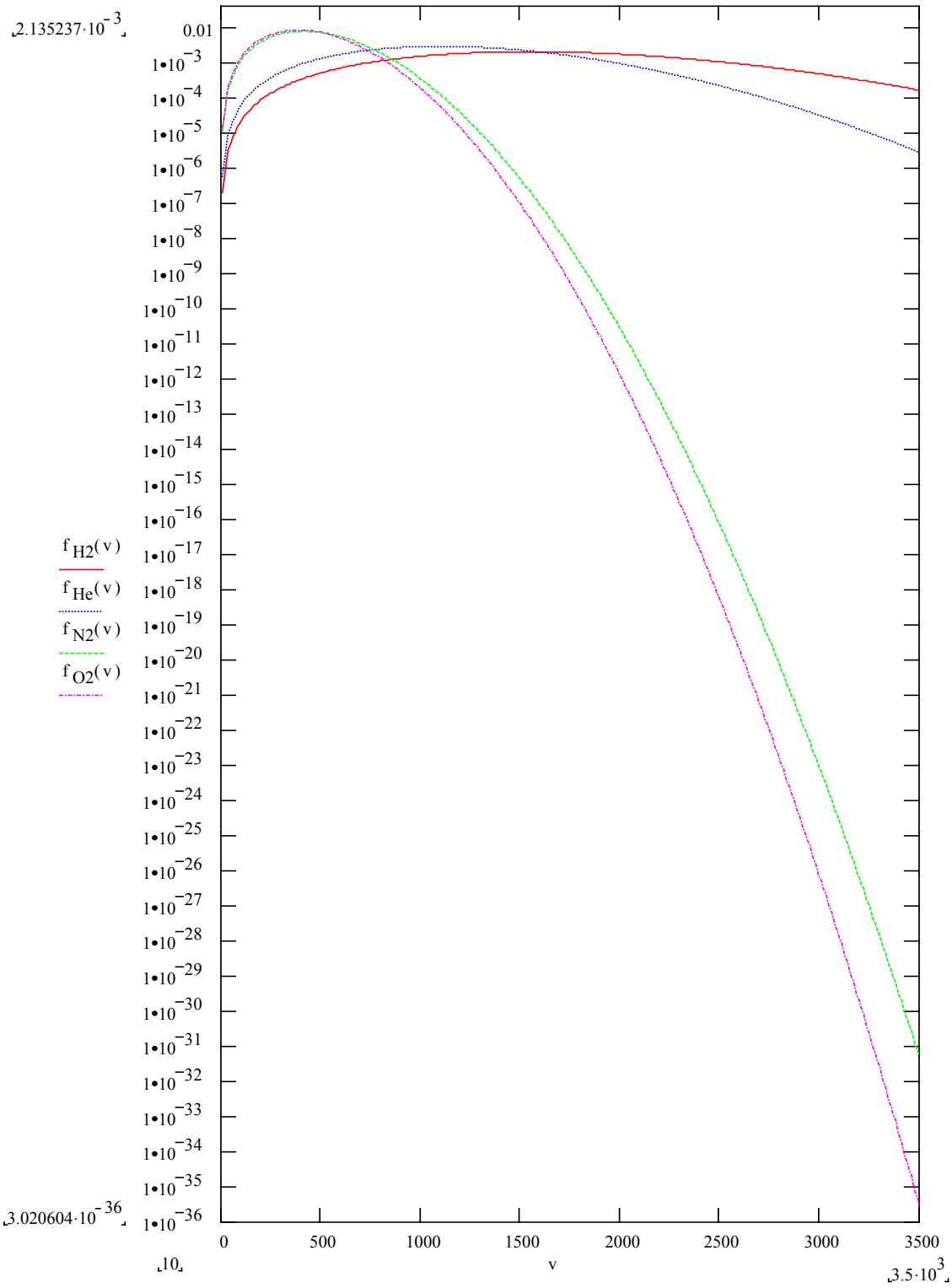

Figure 3: Distribution of velocities for H_2, He, N_2 and O_2 at 293 K

The Doppler shift is given by:

$$f_R = f_S \sqrt{\frac{c - v}{c + v}}$$

where f_R is the frequency observed at the receiver, f_S is the frequency emitted from the source, c is the speed of light and v is the component of the relative velocity along the line of sight between the source and the receiver. In the case of scattering or reflection from a moving object, the Doppler shift is:

$$f_R = f_S \left(\frac{c - v}{c + v} \right)$$

3.7.3 Application to Location of Hydrogen and Helium Leaks

Note that the fraction of molecules in Figure 3 is shown on a logarithmic scale; the fraction of molecules at the higher velocities is many orders of magnitude higher for both H_2 and He than for O_2 or N_2.

The magnitude of the wavelength shift is relatively small compared to the Raman technique: for a wavelength of 633 nm (frequency of 474 THz) and a relative velocity of 1000 m/s the frequency shift is only ~1.6 GHz. This frequency difference could be detected, however, by a heterodyne technique; mixing the backscattered signal with a portion of the transmitted beam on the photodetector. A high pass filter could remove the signal resulting from the slower molecules, leaving only that resulting from the high velocity molecules, which would indicate the presence of lighter molecules such as H_2 or He. Combined with a system that scans the laser source and/or receiver optics could provide an image of the distribution of lighter molecules. Similar systems that measure Doppler shift, known as Doppler lidar systems, are used for measurements of wind speeds. A system that instead measures Doppler broadening rather than Doppler shift might be used to locate leaks of H_2 or He.

3.7.4 Technology Readiness Level

The theory presented here is based on physical principles that are well understood. But we have found no indication of experiments, or even designs for experiments, employing this concept for location of H_2 or He leaks. Thus the technology readiness level is assessed as TRL 1.

3.7.5 Bibliography

None

3.8 Indirect Thermal

3.8.1 Principle of Operation

Solids and liquids emit electromagnetic radiation over a continuum of wavelengths, in contrast to gases, which emit at discrete wavelengths (see section 3.4). The *exitance* (power emitted per unit surface area) of a solid or liquid is a function of the temperature and the emissivity of the material. Objects near room temperature emit primarily in the LWIR (long wave infrared) spectrum (8 – 12 μm.) The total emittance is proportional to the fourth power of the absolute temperature, so measurement of this radiation is a sensitive indicator of temperature. Thus an infrared camera may to used to acquire a *thermal image* of an object.

In many applications the leaking gas may be colder than the ambient temperature, so portion of the pipe or fitting near the leak may become colder than the rest of the pipe or fitting. Even if the gas is stored at ambient temperature, expansion of the gas will cause the gas to cool, and this may lower the temperature of the region of the pipe or fitting near the leak.

3.8.2 Quantitative Model

The exitance M is the power per unit area emitted from a surface. The spectral exitance M_λ is the exitance per unit of spectral bandwidth. For a blackbody (perfect absorber) at an absolute temperature T, the spectral exitance is given by Planck's equation[13]:

$$M_\lambda = \frac{c_1}{\lambda^5 (e^x - 1)}$$

where

$$x = \frac{c_2}{\lambda T}$$

$$c_1 = 2\pi c^2 h = 3.741844 \times 10^4 \qquad [\text{W cm}^{-2}\ \mu\text{m}^{-1}]$$

$$c_2 = \frac{hc}{k} = 1.438769 \qquad [\text{cm K}]$$

For a non-blackbody the exitance is multiplied by the emissivity ε of the surface, which may itself be a function of wavelength. The emissivity is a factor between 0 and 1. For a blackbody ε = 1 for all wavelengths.

The wavelength for which the exitance is a maximum is given by the Wein displacement law[13]:

$$\lambda_{\max} = \frac{2897.756}{T} \qquad [\mu m\ K]$$

Thus the peak exitance from the sun is at visible wavelengths, while the peak exitance from an object at room temperature occurs at far infrared wavelengths (~ 10 μm.)

If one integrates Planck's equation over all wavelengths, the exitance is given by the Stephan-Boltzmann law[13]:

$$M = \sigma T^4$$

where M is the exitance in W/m2, σ is the Stephan-Boltzmann constant, and T is the absolute temperature in Kelvin.

Note the fourth power dependence on temperature. Even a small difference in temperature will result in a relatively large difference in exitance. It is this effect that allows infrared cameras to measure temperature differences with high precision.

3.8.3 Application to Location of Hydrogen and Helium Leaks

This indirect thermal method should be applicable to both H_2 and He, but this depends upon the temperature of the gas. It would naturally be most effective when the gas is cold (i.e. stored as a liquid.) Far-infrared cameras are available off-the-shelf with the ability to detect temperature variations as small as 0.03 K. Thus the temperature resolution of the camera technology is not expected to be a limiting factor for this approach. In practice there will be variations in the temperature and emissivity of the pipe or fitting even in the absence of a leak, and this background clutter is expected to be the primary limitation on the effectiveness of this technique. Experience with the failure of this technique to detect small leaks suggests that only relatively large leaks can be located with this technique[12].

3.8.4 Technology Readiness Level

Infrared cameras suitable for this application are available off-the-shelf. But we have no information indicating that this technique has been used to locate leaks. Therefore the readiness is assessed as TRL 3.

3.8.5 Bibliography

- William L. Wolfe, "Radiation Theory", *Sources of Radiation*, George J. Zissis *ed.*, Bellingham: SPIE press (1993).
- "Infrared Cameras", http://www.indigosystems.com/cameras.html

3.9 Rayleigh Intensity

3.9.1 Principle of Operation

The elastic scatter of light from atoms and molecules is termed Rayleigh scatter. The intensity of Rayleigh scattered light is a function of the wavelength and the refractive index of the gas or other scattering media. Thus a measure of the fraction of flux that is scattered from a laser beam passing through a gas, is a measure of the index of refraction, which in turn is a property of the gas. In this approach, the scattered radiation is typically observed at an angle of 90° to the incident laser beam, but could in principle be observed at any angle.

3.9.2 Quantitative Model

The intensity of Rayleigh scattering is usually described by defining an angular cross-section σ for each individual molecule as the scattered power per unit solid angle (intensity) divided by the incident power per unit area (irradiance). For a gas of number density N the angular cross-section is related to the index of refraction by:

$$\sigma(90°) = \frac{4\pi^2 (n-1)^2}{N^2 \lambda^4}$$

where n is the index of refraction of the gas and λ is the wavelength of the light.

The refractive indices of standard air, pure H_2, and pure He, at 20 C and 1 atm are given in Table 4.

Table 4: Refractive Index for pure Air, H_2, and He

Gas	Refractive Index at 1 atm, 20°C
air	1.000274
H_2	1.000122
He	1.000033

The refractive index for a mixture of gases is given by[14]:

$$n_{mix} - 1 = \sum_i k_i \rho_i$$

where: n_{mix} is the index of refraction for the mixture k_i is the Gladstone-Dale constant for each species (k_{air} = 0.000226 m^3/kg, k_{H2} = 0.00147 m^3/kg, k_{He} = 0.000201m^3/kg) , and ρ_i is the density of the species in the kg/m^3.

Pressure and temperature also affect the index of refraction, so a more general formulation is:

$$n_{mix} - 1 = \frac{P}{\bar{R}\,T} \sum_i k_i X_i M_i$$

where P is the pressure, $\bar{R}$ is the universal gas constant, T is the temperature, X_i is the species mole fraction, and M_i is the molecular weight of the species.

3.9.3 Application to Location of Hydrogen and Helium Leaks

The Rayleigh cross-section depends upon the value of $(n-1)^2$, and (n-1) is appreciably different for air, H_2 and He (see Table 4). But suspended particles will also scatter light, by Mie scattering, which is much more efficient than Raleigh scattering. This technique has been used to measure gas concentrations in jets, but in these experiments the gases have been filtered to remove particulates.

3.9.4 Technology Readiness Level

This technique has been demonstrated in application to determining the concentration of gases in a jet with a precision of 2% in a laboratory environment[15], but we have found no indication of application to leak location. So for H_2 and He leak location, this technique is assessed as TRL 3.

3.9.5 Bibliography

- W.M. Pitts, "Effects of global density ratio on the centerline mixing behavior of axisymmetric turbulent jets", *Experiments in Fluids,* 11, Pp. 125-134 (1991). (see Appendix 6.2.10)
- W.M. Pitts and T. Kashiwagi, "The application of laser-induced Rayleigh light scattering to the study of turbulent mixing", *J. Fluid Mech*, **141**, Pp 391-429. (see Appendix 6.2.11)
- F.C. Gouldin, R.W. Schefer, S.C. Johnson and W. Kollmann, "Nonreacting Turbulent Mixing Flows", *Prog. Energy Combust. Sci.*, **12**, Pp. 257-303 (1986). (see Appendix 6.2.12)

3.10 Schlieren Imaging

3.10.1 Principle of Operation

The refractive index of a gas is a property of the gas, and is also varies with temperature and pressure. When light passes between regions of differing refractive indices it is deflected. This process is known as refraction. The 'shimmer' observed when viewing across a hot object, such as a roadway is an example of this effect.

Schlieren imaging uses this effect to produce an image of refractive index variations. In the *Ronchi schlieren* version of this approach[16,17] the region of interest is illuminated and viewed through a Ronchi ruling (essentially a high-contrast stripe pattern that is alternates transparent and opaque stripes). A curved mirror placed on the opposite side of the region of interest reflects an image of the Ronchi ruling back upon itself. The system is aligned such that the transparent stripes in the image line up with the transparent stripes on the original, and the image of the region appears bright. If the light is deflected in the region between the illuminator/camera and the mirror, then the transparent stripes in the image of the ruling line up with the opaque stripes in the original, and corresponding region will appear dark in the camera image. The sensitivity to refraction is a function of the distance from the source of the refraction to the mirror. The highest sensitivity is achieved nearest to the mirror.

Another variation on this technique, known as *zebra schlieren*, replaces the mirror with a reflecting cloth background that is directly imprinted with alternating reflective and absorbing stripes, and this is illuminated with a light source[16]. Or a special projector may be used to illuminate an existing background with a striped pattern. The advantage of this variation is that the cloth or projector may be more portable than the large mirror required for the standard technique. For zebra schlieren, the highest sensitivity is obtained in the region nearest to the camera, and the poorest sensitivity is obtained in the region near the background.

3.10.2 Quantitative Model

Quantitative models of the sensitivity of this technique to variations in refractive index exist in the literature[18]. The refractive indices of standard air, pure H_2, and pure He, at 20 C and 1 atm are given in Table 5.

Table 5: Refractive Index for pure Air, H_2, and He

Gas	Refractive Index at 1 atm, 20°C
air	1.000274
H_2	1.000122
He	1.000033

The refractive index for a mixture of gases is given by[14]:

$$n_{mix} - 1 = \sum_i k_i \rho_i$$

where: η_{mix} is the index of refraction for the mixture k_i is the Gladstone-Dale constant for each species (k_{air} = 0.000226 m^3/kg, k_{H2} = 0.00147 m^3/kg, k_{He} = 0.000201m^3/kg) , and ρ_i is the density of the species in the kg/m^3.

Pressure and temperature also affect the index of refraction, so a more general formulation is:

$$n_{mix} - 1 = \frac{P}{\bar{R}T} \sum_i k_i X_i M_i$$

where P is the pressure, $\bar{R}$ is the universal gas constant, T is the temperature, X_i is the species mole fraction, and M_i is the molecular weight of the species.

3.10.3 Application to Location of Hydrogen and Helium Leaks

While the minimum detectable concentration of H_2 or He may depend on the minimum detectable variation in index of refraction, in practice the sensitivity of this technique may be limited by the clutter (or false signal) caused by variations in refractive index resulting from variations in the *temperature* of the ambient air. Table 6 shows the equivalence between temperature variations in air with no H_2 or He, and the concentrations of H_2 or He, that would cause the same change in refractive index.

Table 6: Temperature variations and H_2 or He concentrations that cause equivalent changes in refractive index

Temperature Variation	Equivalent concentration of H_2 [ppm]	Equivalent concentration of He [ppm]
0.1°	34	46
0.3°	104	138
1.0°	346	461
3.0°	1049	1391

3.10.4 Technology Readiness Level

Schlieren imaging techniques for leak location have been demonstrated in a laboratory environment at KSC. So the readiness level is assessed as TRL 4.

3.10.5 Bibliography

- H. Sandner, "Introduction to the Schlieren and Shadowgraph Method" Pp. 11-23 in *Optical Measurements: Techniques and Applications*, Franz Mayinger *ed.*, New York: Springer-Verlag (1994).
- Anli K. Shenoy, Ajay K. Agrawal and Subramanyam R. Gollahalli, "Quantitative Evaluation of Flow Computations by Rainbow Schlieren Deflectometry", *AIAA Journal,* **36**, No.11, Pp. 1953-1960 (Nov, 1998). (see Appendix 6.2.13)
- R.E. Peale and P.L. Summers, "Zebra schlieren optics for leak detection", *Applied*

Optics, **35**, No.22, Pp. 4518 – 4521 (Aug., 1996). (see Appendix 6.2.14)

- O.Kafri, "Noncoherent method for mapping phase objects", *Optics Letters,* **5**, Pp. 555 – 557 (Dec.,1980). (see Appendix 6.2.15)
- "Toepler's Schlieren Method: Basic principles for its use and quantitative evaluation", *Selected Papers on Schlieren Optics*, Jurgen R. Meyer-Arendt *ed.*, SPIE Milestone Series, **MS61** (1992). (see Appendix 6.2.16)
- Norman F. Barnes and S. Lawarence Bellinger (1945), "Schlieren and Shadowgraphy Equipment for Air Flow Analysis", *Selected Papers on Schlieren Optics*, Jurgen R. Meyer-Arendt *ed.*, SPIE Milestone Series, **MS61** (1992). (see Appendix 6.2.17)
- Edward B. Temple, "Quantitative Measurement of Gas Density by Means of Light Interference in a Schlieren System", *Selected Papers on Schlieren Optics*, Jurgen R. Meyer-Arendt *ed.*, SPIE Milestone Series, **MS61** (1992). (see Appendix 6.2.18)
- L.A. Yates, "Constructed interferograms, schlieren and shadowgraph: a user's manual", *NASA CR-194530* (1993). (see Appendix 6.2.19)
- K.Al-ammar, A. K. Agrawal, S. R. Gollahalli, Devon Griffin, "Application of rainbow schlieren deflectometry for concentration measurements in an axisymmetric helium jet", *Experiments in fluids,* **25**, No 2, Pp. 89 – 95 (1998). (see Appendix 6.2.20)

3.11 Shearography

3.11.1 Principle of Operation

Shearography encompasses a number of different implementations, including s*hearing interferometry* and *electronic speckle pattern shearing interferometry (ESPI.)* The basic principle, however, is common to all these implementations. Two coherent (laser) beams are made to interfere, and the degree of interference is a measure of the difference in the optical path length traveled by the two beams. *Optical* path length is the product of the geometric distance and the index of refraction of the medium through which the light travels.

A camera is used to display the interference pattern, and changes in this pattern are processed to display changes in the optical path difference between the beams. In some implementations, both beams are projected onto a remote surface[19]; in others only one beam is incident on the background while the second beam is mixed with the first at the detector[20]. If the surface is rough, this will produce a *speckle* pattern.

If the shape of the surface changes, this alters the optical path lengths and these changes are manifested in the interference pattern captured by the camera. Shearography systems are often used to measure deformations of a surface using this technique. However, since optical path length depends on the refractive index of the intervening medium, this approach can also be used to detect changes in the refractive index of a gas or mixture of gases. In this case the background surface is expected to remain fixed, so that observed variations in the interference pattern are known to be due to refractive index variations in the gas.

It is also possible to project a single or dual beam directly from a source to the camera without reflecting from a rough background. In this case the interference pattern will not produce *speckle*.

3.11.2 Quantitative Model

In principle shearography can be extremely sensitive. A change in optical path length of only one-half of the wavelength of the light is all that is required to change the degree of interference all the way from constructive (bright) to destructive (dark.) Detailed mathematical models are available in references on this topic[19].

3.11.3 Application to Location of Hydrogen and Helium Leaks

As is the case for the Rayleigh intensity technique (section 3.9) and the schlieren technique (section 3.10), this approach is highly sensitive and performance is expected to be ultimately limited by clutter rather than by the sensitivity. Variations in refractive index can be caused by variations in the temperature of the ambient air as well as by the addition of H_2 or He as discussed for the schlieren technique (section 3.10.3). It may be possible to distinguish a leak based on context (i.e. the shape and location of the disturbance), but the extent to which this is feasible will depend on the operational environment.

3.11.4 Technology Readiness Level

Complete systems for ESPI are commercially available. Such a system has been tested at KSC, so the technology readiness level is assessed as TRL 5.

3.11.5 Bibliography

- Brad A. VanDerWege, Christopher J. O'Brien and Simone Hochgreb, "Quantitative shearography in axisymmetric gas temperature measurements", *Optics and Lasers in Engineering,* **31**, Pp.21-39 (1999). (see Appendix 6.2.21)
- E.A.Abd El-Ghafar and H.El-Ghandoor, "Detection of vibrating sound fields using speckle shearography", *Current Developments in Vibration Control for Optomechanical Systems, SPIE Proceedings*, **3786**, Pp. 126-133 (1999). (see Appendix 6.2.22)

4 DIFFUSION MODEL

In order to evaluate the various technologies for leak location, it is desirable to have a model (or map) of concentration of H_2 or He as a function of leak rate, distance from the leak, and time since the leak initiated. For the case of a leak into an open area, the concentration follows the differential equation:

$$\frac{\partial C(r,t)}{\partial t} = D\frac{1}{r^2}\frac{\partial}{\partial r}(r^2\frac{\partial C(r,t)}{\partial r})$$

where C is the concentration in mol/m^3, D is the diffusion coefficient, r is the radius from the leak, and t is the time since initiation of the leak. With appropriate boundary conditions:

$$C(r,t) = 0 \quad \text{for } t<0$$
$$C(r,0) = \delta(r)$$
$$C(\infty,t) = 0$$

where δ is the *Kronecker delta* function, the solution[21] is:

$$C(r,t) = \frac{\phi}{4\pi Dr}\,efrc\,[\frac{r}{\sqrt{4Dt}}]$$

where ϕ is the leak rate in mol/s, and *erfc* is the complimentary error function[22]:

$$erfc(x) = \frac{2}{\sqrt{\pi}}\int_x^\infty e^{-\xi^2}d\xi$$

An interactive version of this model has been provided in the form of a *MathCAD* worksheet.

For the steady state case $t\rightarrow\infty$ and the concentration reduces to:

$$C(r) = \frac{\phi}{4\pi Dr}$$

The diffusion coefficients for gas 1 in gas 2 is given by[23]:

$$D_{1,2} = \frac{0.604 \times 10^{-8} \bullet T^{1.81} \bullet \left[\frac{M_1 + M_2}{M_1 M_2} \right]^{0.5}}{p\left(T_{c,1} T_{C,1}\right)^{0.1405} \left(V_{c,1}^{0.4} + V_{c,2}^{0.4}\right)^2}$$

where:

M_1, M_2 : molecular weight of both components in kg/kmol;

$T_{c,1}$, $T_{c,2}$: critical temperature in K;

$V_{c,1}$, $V_{c,2}$: critical volume in m^3/kmol ($V_c = M/(1000 d_c)$)

T: temperature in K;

P: pressure in bar (1bar = 0.98692 atm) ;

$D_{1,2}$: diffusion coefficient of gas 1 in gas 2 in m^2/s

The critical properties for selected gases[24] are given in Table 7:

Table 7: Critical data for selected gases

Gas	T_c [K]	P_c [bar]	d_c [g cm^{-3}]	MW [kg $kmol^{-1}$]
air	132	3.77	0.316	29
H_2	33.2	1.29	0.031	2.02
He	5.19	0.23	0.070	4.003
N_2	126.2	3.39	0.313	28.01
O_2	154.7	5.04	0.436	32.00
CO_2	31	7.38	0.468	44.0

Therefore, at a temperature of 25°C and pressure of 1 atm:

$$D_{H2\text{-}Air} = 7.78 \text{ x } 10^{-5} \text{ m}^2/\text{s}$$

$$D_{He\text{-}Air} = 7.73 \text{ x } 10^{-5} \text{ m}^2/\text{s}$$

An interactive diffusion model has been developed using MathCAD. Sample results from this model are given in Figure 4, which shows the molar fraction in percent (equivalent to percent concentration by volume) as a function of distance from the leak for an H_2 leak at 10^{-2} SCIM after 1 s, 1 min, 1 h, and for steady state. The concentration is linearly proportional to the leak rate, so the *form* of the curves is the same for all leak rates; changing the leak rate effectively changes only the scale of the y axis. The diffusion coefficient for He is very close to that for H_2, so the graph for He is virtually the same.

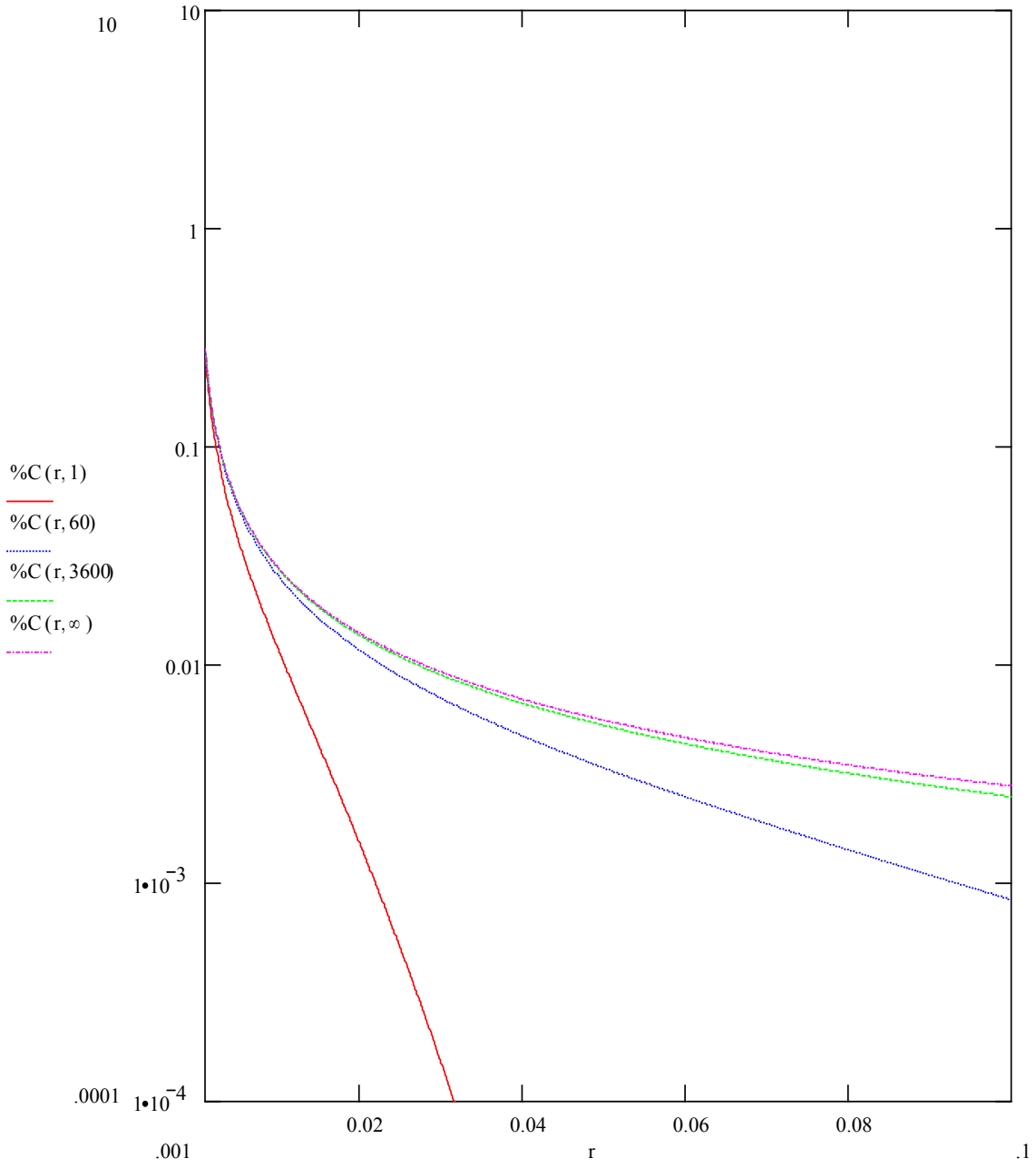

Figure 4: Concentration of H_2 [mol fraction] vs. distance [m] for a leak of 10^{-2} SCIM, at 1 s, 1 min, 1 h, and steady state

5 REFERENCE CITATIONS

[1] Youngquist, et al. "Ultrasonic imaging system", United States Patent: 5,979,239. November 9, 1999. (see Appendix 6.2.1)

[2] Youngquist, et al. "Ultrasonic leak detection system", United States Patent: 5,710,377. January 20, 1998. (see Appendix 6.2.2)

[3] Gerhard Herzberg, F.R.S. 1989, *Molecular Spectra and Molecular Structure: Volume I. Spectra of Diatomic Molecules,* 2nd Edition, p.54 & p.279, Malabar: Krieger.

[4] Owen Willans Richardson, *Molecular Hydrogen and Its Spectrum,* p. 65, New Haven: Yale University Press.

[5] Gerhard Herzberg, 1944, *Atomic Spectra and Atomic Structure*, 2nd Edition, p.64, New York: Dover.

[6] "Evaluation of Raman Lidar For Hydrogen Detection", NASA Report # 802841. (see Appendix 6.2.5)

[7] Wim A. de Groot, "The use of Spontaneous Raman Scattering for Hydrogen Leak Detection", NASA CR 195373, AIAA-94-2983 (1994). (see Appendix 6.2.4)

[8] B. Caputo, "Hydrogen Detection Lidar," Computer Genetics Corporation, VEN-1519, Final Report NASA Contract #NAS10-11421 (1988).

[9] "Raman Lidar Testing at JSC, DRAFT", (Nov. 5, 1990). (see Appendix 6.2.7)

[10] *Chemical Applications of Nonlinear Raman Spectroscopy*, Albert B. Harvey *ed.*, p. 31, Naval Research Laboratory: Washington, D.C. (1981).

[11] P.R. Regnier, and J.P.-E.Taran, "On the possibility of measuring gas concentrations by stimulated anti-Stokes scattering", *Appl. Phys. Lett.,*Vol.23, No. 5, p. 240 (1973). (see Appendix 6.2.9)

[12] Robert Youngquist, private communication.

[13] William L. Wolfe, "Radiation Theory" in *Sources of Radiation*, Pp.8-12, George J. Zissis *ed.*, Bellingham: SPIE press (1993).

[14] L.A. Yates, "Constructed interferograms, schlieren and shadowgraph: a user's manual", *NASA CR-194530*, (1993). (see Appendix 6.2.19)

[15] F.C. Gouldin, R.W. Schefer, S.C. Johnson and W. Kollmann, "Nonreacting Turbulent Mixing Flows", *Prog. Energy Combust. Sci.*, **12**, Pp. 257-303 (1986). (see Appendix 6.2.12)

[16] R.E. Peale and P.L. Summers, "Zebra schlieren optics for leak detection", *Applied Optics*, **35**, Pp. 4518 – 4521 (Aug., 1996). (see Appendix 6.2.14)

[17] O.Kafri, "Noncoherent method for mapping phase objects", *Optics Letters,* **5**, Pp. 555 – 557 (Dec., 1980). (see Appendix 6.2.15)

[18] "Toepler's Schlieren Method: Basic principles for its use and quantitative evaluation", *Selected Papers on Schlieren Optics*, Jurgen R. Meyer-Arendt *ed.*, SPIE Milestone Series, **MS61** (1992). (see Appendix 6.2.16)

[19] E.A.Abd El-Ghafar and H.El-Ghandoor, "Detection of vibrating sound fields using speckle shearography", *SPIE,* Vol. 3786, Pp. 126 (1999). (see Appendix 6.2.22)

[20] Brad A. VanDerWege, Christopher J. O'Brien and Simone Hochgreb, "Quantitative shearography in axisymmetric gas temperature measurements", *Optics and Lasers in Engineering,* **31**, Pp.21-39 (1999). (see Appendix 6.2.21)

[21] H.S.Carslaw and J.C. Jaeger, *Conduction of Heat in Solids, 2nd ed.*, p. 261, Oxford (1959).

[22] J. Crank, *The Mathematics Of Diffusion*, p. 19 & Table 2.1, Oxford (1964).

[23] http://chemengineer.about.com/science/chemengineer/library/weekly/aa072197.htm

[24] H.W. Liepmann and A. Roshko, *Elements of Gasdynamics*, John Wiley & Sons: New York (1957).

6 APPENDICES

6.1 NASA Technology Readiness Levels

Level 1	Basic principles observed and reported
Level 2	Technology concept and/or application formulated
Level 3	Analytical & experimental critical function and/or characteristic proof-of-concept
Level 4	Component and/or breadboard validation in laboratory environment
Level 5	Component and/or breadboard validation in relevant environment
Level 6	System/subsystem model or prototype demonstration in relevant environment
Level 7	System prototype demonstration in relevant environment
Level 8	Actual system completed and “Flight Qualified” through test and demonstration
Level 9	Actual system “Flight Proven” through successful mission operations

6.2 Selected Papers

Copies of the following papers are included in this appendix. The index tabs correspond to the last digits in the heading number.

6.2.1 Ultrasonic imaging system

6.2.2 Ultrasonic leak detection system

6.2.3 Tracking Gas Leaks With Active IR Scanning

6.2.4 The use of Spontaneous Raman Scattering for Hydrogen Leak Detection

6.2.5 Evaluation of Raman Lidar For Hydrogen Detection

6.2.6 Lidar Hydrogen Detection Test

6.2.7 Raman Lidar Testing at JSC, DRAFT

6.2.8 A Review of the Theory and Application of CARS

6.2.9 On the possibility of measuring gas concentrations by stimulated anti-Stokes scattering

6.2.10 Effects of global density ratio on the centerline mixing behavior …

6.2.11 The application of laser-induced Rayleigh light scattering to the study of turbulent mixing

6.2.12 Nonreacting Turbulent Mixing Flows

6.2.13 Quantitative Evaluation of Flow Computations by Rainbow Schlieren Deflectometry

6.2.14 Zebra schlieren optics for leak detection

6.2.15 Noncoherent method for mapping phase objects

6.2.16 Toepler's Schlieren Method: Basic principles for its use and quantitative evaluation

6.2.17 Schlieren and Shadowgraphy Equipment for Air Flow Analysis

6.2.18 Quantitative Measurement of Gas Density … in a Schlieren System

6.2.19 Constructed interferograms, schlieren and shadowgraph: a user's manual

6.2.20 Application of rainbow schlieren deflectometry for concentration measurements …

6.2.21 Quantitative shearography in axisymmetric gas temperature measurements

6.2.22 Detection of vibrating sound fields using speckle shearography